

Full length article

Influence of sulfur addition on the glass formation, phase transformation and mechanical properties of Cu₅₀Zr₅₀ alloy

Hao-Ran Jiang^a, Jing-Yi Hu^b, Nico Neuber^b, Maximilian Frey^b, Lin-zhi Xu^c, Kang Sun^c, Yan-Dong Jia^c, Gang Wang^{c*}, Ralf Busch^b, Jun Shen^d

^a Materials Genome Institute, Shanghai University, Shanghai 200444, China

^b Chair of Metallic Materials, Saarland University, Campus C6.3, Saarbrücken 66123, Germany

^c Institute of Materials, School of Materials Science and Engineering, Shanghai University, Shanghai 200444, China

^d College of Mechatronics and Control Engineering, Shenzhen University, Shenzhen 518060, China

ARTICLE INFO

Keywords:

Bulk metallic glasses
Crystallization
Sulfur addition
Glass-forming ability
Mechanical properties

ABSTRACT

In this work, a thorough study on the effects of sulfur-addition in the Cu₅₀Zr₅₀ glass-forming system was conducted using laboratory-based X-ray diffraction (XRD), synchrotron-based high-energy XRD (HESXRD), differential scanning calorimetry, and uniaxial compression testing. We report that the glass-forming ability (GFA), thermal stability, phase transformation sequence during heating and cooling, as well as the mechanical properties of the Cu₅₀Zr₅₀ system are highly sensitive to the sulfur concentration. Proper addition of sulfur can not only stabilize the B2-CuZr phase, but also enhances the GFA of the system. This enables the formation of BMG composites that solely contain a B2 phase, which results in a combination of high strength and substantial plastic strain under compressive loading. The total strains of the newly developed BMG composites with sulfur contents of 0.5 and 1.0 at.% are as large as ~10 at.%, exceeding the previously reported strains of the Cu₅₀Zr₅₀ BMG by far. These superior properties make the Cu-Zr-S BMG composites a promising candidate material for industrial applications. In addition, it is found that excessive addition of sulfur leads to the precipitation of the Cu₁₀Zr₇ phase upon cooling from the alloy melt and a sulfide phase during heating from the glassy state. HESXRD experiments suggest that the preferential bonding between Zr and S atoms could be the determining structural mechanism on the atomic scale, leading to the changing primary crystallization sequence for heating and cooling. The findings in this work further strengthen the high relevance of sulfur in alloy development and tuning of properties in BMGs, especially considering the low cost, good availability, and non-toxicity of sulfur in the relevant modifications.

1. Introduction

Since the discovery of bulk glass formation in the binary Cu-Zr system in 2004, the alloy system quickly attracted considerable attention in the research community because of its scientific and industrial significance [1–3]. The development of Cu-Zr binary bulk metallic glasses (BMGs) relativizes the widely held point of view of BMGs necessarily being multi-component systems that consist of more than three elements [4]. The Cu-Zr system combines high glass-forming ability (GFA) with simple components, thus being a perfect candidate for the study of many fundamental scientific issues related to amorphous solids, such as the GFA, atomic structure, relaxation behavior, and the glass transition, especially by means of atomic-scale computational simulations [5–8].

Extensive research on the fundamental properties of the Cu-Zr binary system has been conducted in the past decades. The knowledge obtained from these studies leads to a deeper understanding on the nature of metallic glasses and make the Cu-Zr system one of the most well-known alloy systems in the metallic glass community [6–12]. In addition to its significant research value, the binary system is also promising for industrial applications as a structural material, as it combines many desirable characteristics, i.e., low cost, high strength, distinct compressive ductility, and non-toxicity [13–15].

Minor additions play an essential role in the compositional design and property modification of BMGs [16]. For the Cu-Zr system, additions of some metal elements, like Al, Ag, and Ti, have been found to favor the glass formation, resulting in a substantial increase in the critical casting

* Corresponding author.

E-mail address: g.wang@shu.edu.cn (G. Wang).

diameter from ~ 2 mm to up to above 10 mm [17–21]. Besides the improvement of the GFA, considerable attention was also paid to find additions that stabilize the B2-CuZr phase in the binary system during rapid quenching, which would facilitate the synthesis of B2 phase-reinforced CuZr-based glass-crystal composites [22]. Upon loading, the stress can induce a martensitic phase transformation of the B2 phase, leading to macroscopically plastic deformation and work hardening of the BMG composites [23–26]. However, fabrication of CuZr-based BMG composites containing only the B2 phase is still quite challenging, as this well-known ordered cubic phase is only thermodynamically stable at high temperatures. Hence below 1002 K the B2 phase decomposes into the low-temperature equilibrium phases Cu₁₀Zr₇ and CuZr₂, according to the Cu-Zr binary phase diagram [27]. Recent studies have shown that micro-alloying with some metal elements, such as Co, Ag, Zn, Ti, and Ni, influences the stability of the B2 phase [22]. This allows to manipulate the microstructure and properties of the CuZr-based BMG composites. In fact, both aforementioned research topics, GFA and BMG composites, are attributed to the crystallization of glass-forming liquids during solidification. Apart from the crystallization upon cooling, which is determining the GFA, the crystallization during heating from the glassy state is important as well. It is especially crucial for the post-processing of BMGs in their supercooled liquid region (SLR), where the BMGs regain their fluidity and can be processed like plastics through thermoplastic forming techniques [28,29]. Another processing route is additive manufacturing (AM), i.e., 3D-printing of BMG, in which the crystallization of the glassy phase plays an important role. In AM the repetitive heat accumulation during the layer-by-layer process may cause crystallization of the initially formed amorphous parts in the heat-affected zones, which of course is detrimental to the mechanical properties of the 3D-printed BMGs in general [30,31].

The non-metallic element sulfur is commonly known to cause catastrophic failure in conventional crystalline metals or alloys [32,33]. However, some recent works reported that sulfur can be an alternative alloying element in the case of amorphous alloys, which is contrary to the traditional cognition for crystalline metal materials [34–36]. Sulfur can not only stabilize the alloy's liquid phase, thus promoting the glass formation during solidification, but can also positively alter the properties of BMGs [36,37]. Since sulfur is easily available and widely used in industry, the development of sulfur-containing BMGs may accelerate the widespread applications of BMGs as structural materials. Therefore, studying the influence of sulfur on the glass formation, phase stability, and various properties of BMGs and the underlying mechanisms are of great importance for popularizing the use of sulfur in metallic glasses.

In the present work, a thorough study of the sulfur-addition effects on the Cu₅₀Zr₅₀ BMGs is conducted using a selection of laboratory and synchrotron-based techniques, such as differential scanning calorimeter (DSC), conventional X-ray diffraction (XRD), high-energy synchrotron XRD (HESXRD) and uniaxial compression testing. The GFA, phase formation sequence upon quenching and heating, as well as mechanical properties of the studied BMGs are revealed to be highly dependent on the sulfur concentration. In particular, it is found that an appropriate addition of sulfur can not only improve the GFA of the studied alloys, but also stabilize the CuZr cubic B2 phase, thus facilitating the manufacturing of B2 phase-reinforced CuZr-based BMG composites, which exhibit high strength in combination with significant plastic deformation under compressive loading. Overall, the findings in this work further suggest that sulfur might be an effective microalloying element for BMGs and that its use deserves to be extended to more alloy systems.

2. Experimental

2.1. Sample preparation

Master alloys with nominal compositions of (Cu₅₀Zr₅₀)_{100-x}S_x ($x = 0, 0.5, 1.0, 1.5, 2.0, 2.5, 3.0, 3.5, 4.0$, at.%, hereafter CuZrS_x) were

produced by arc-melting the raw metals Cu and Zr and the pre-alloy Cu₂S with purities higher than 99.9 wt.% under a Ti-gettered Ar atmosphere. To ensure the chemical homogeneity of the alloys, each ingot was flipped and remelted at least five times. Cylindrical samples with diameters of 2 mm and 3 mm and plate-shaped samples with a thickness of 0.5 mm were produced by sucking the remelted alloy melts into water-cooled copper molds with different cavities. Samples for further structural, thermodynamical, and mechanical experiments were cut from these as-cast samples.

2.2. Structural characterization

The amorphous and crystalline structures of the as-cast CuZrS_x samples were analyzed by XRD in a PANalytical X'Pert Pro-diffractometer using Cu-K α radiation. As different parts of the sample experience varying cooling rates during the casting process, the transverse cross-sections of the center part of the 2 mm and 3 mm rod-shaped samples were used for XRD measurements. For plated-shaped samples with a thickness of merely 0.5 mm, the samples were ground in the thickness direction to half of its original thickness for XRD analysis. Only amorphous samples verified by conventional XRD were used in the HESXRD experiments, which were conducted at the beamline P21.1 residing at PETRA III of the German Electron Synchrotron (DESY). X-rays with a wavelength of ~ 0.1220 Å were used in transmission geometry for data acquisition. During the *in-situ* diffraction experiments, as-cast samples were heated at 0.333 K/s in a Linkam THMS 600 furnace under the protection of a flow of high purity argon (99.999 wt%). The acquisition time for each diffraction pattern was 5 s, resulting in a temperature resolution of ~ 1.67 K. For data processing, the raw 2D diffraction pattern recorded by a Perkin Elmer XRD1621 detector was corrected and azimuthally integrated using the PyFai software. The obtained diffraction intensity $I(Q)$ allows a detailed characterization of the phase transformation process of the CuZrS_x BMGs upon heating. The background subtraction and calculation of total structure factor $S(Q)$ and the reduced pair distribution function $G(r)$ from the raw intensity data was performed using the PDFgetX2 software [38].

2.3. Calorimetric measurements

Calorimetric measurements were performed using the PerkinElmer DSC 8000 (323–973 K) and the Netzsch DSC 404F3 (323–1373 K) for the determination of the glass transition, crystallization, solid phase transformation, and melting behavior of the as-cast samples. Both instruments were calibrated using the melting points and heats of fusion of pure metals such as In, Zn, Al, Ag and Au in the relevant temperature ranges and for the applied heating rate. All the measurements were carried out at a heating rate of 0.333 K/s under a constant flow of high-purity Ar. The enthalpy of crystallization ΔH_x of the as-cast samples was evaluated by integrating the crystallization peak in the DSC curves. A comparison of the ΔH_x between the partially crystallized and fully amorphous samples allows for an approximate assessment of the volume fraction of amorphous phase, being a measure of the GFA of the CuZrS_x alloys.

2.4. Mechanical tests

Cylindrical samples with a diameter of 2 mm and a length of 4 mm were used for the compression tests, which were carried out in an Instron mechanical testing machine at an engineering strain rate of 1×10^{-4} s⁻¹. To verify the reproducibility of the data, at least three samples of each alloy were tested. The engineering strain of the samples was calibrated by compressing the WC-Co hard metal plates with no sample in between to eliminate the influence of machine displacement.

3. Results

3.1. Glass-forming ability and phase formation upon quenching

The GFA and the crystalline phases formed upon quenching of the newly developed sulfur-containing CuZr-based alloys are determined using XRD and DSC. As shown in Fig. 1(a), the $I(Q)$ profiles of the 500 mm-thick CuZrS_x ($x = 0, 1.0, 2.0, 3.0, 4.0$, at.%) samples, acquired using the state-of-the-art HESXRD technique, exhibit the typical diffractogram observed for glassy samples, with a significant main peak, followed by a second peak that exhibits a shoulder. Correspondingly, the DSC traces of the 500 mm plates in Fig. 2(a) show the distinct endothermal signal associated with the glass transition followed by exothermic peaks typical for crystallization, further confirming the amorphous structure of the 500 mm as-cast samples. For the rod-shaped samples with a diameter of 2 mm, however, Bragg peaks emerge in the diffraction patterns of the CuZrS_x samples [Fig. 1(b)]. This indicates that the decreased cooling rate, due to the increased sample size of 2 mm, is not sufficient to completely suppress the formation of crystalline phases during the casting process. Although all five samples are partially crystalline, an indication of the GFA of the studied alloys can still be deduced from the intensity of the Bragg reflections as displayed in Fig. 1(b). Clearly, the $\text{CuZrS}_{1.0}$ and $\text{CuZrS}_{3.0}$ samples show the least pronounced reflexes, indicating a smaller crystalline fraction and suggesting a superior GFA for these two alloys within the series. To evaluate the GFA of the CuZrS_x alloys in more detail, calorimetric measurements were conducted to determine the crystallization enthalpy, DH_x , of the 2 mm rod samples by integration over the respective exothermal event [Fig. 2(b)]. A comparison of the DH_x of the fully amorphous (500 mm) and partially crystallized (2 mm) samples leads to a quantitative determination of the volume fraction of amorphous phase, V_{glass} , in the rod samples. As summarized in Fig. 3 and Table 1, minor sulfur additions with $S \leq 3$ at.% can stabilize the glassy phase upon quenching, reflected by the significant increase in V_{glass} from merely 19 % of the base alloy to above 90 % of alloys with $1.0 \leq S \leq 3.0$ at.%. Interestingly, two V_{glass} maximums are reached at the sulfur content of 1.0 and 3.0 at.%, which is in good agreement with the XRD results. This further confirms the highest GFA of these two alloys. A further increase of the S concentration to above 3 at.% results in a dramatic decline of V_{glass} approaching to values of the base alloy (Table 1). In the following the complicated variation of GFA

with increasing sulfur content will be discussed with respect to the change in the crystallization sequence during cooling.

XRD patterns for the partially crystallized samples, as exhibited in Fig. 1(b) and (c), reveal that the crystalline product of the studied alloy series is strongly dependent on the composition. The dominant crystalline phase of the 2 mm $\text{Cu}_{50}\text{Zr}_{50}$ sample is identified to be monoclinic CuZr [Fig. 1(b)]. The $\text{Cu}_{51}\text{Zr}_{14}$ phase, which was observed by Yu et al. [17] in the as-cast $\text{Cu}_{50}\text{Zr}_{50}$ sample, can also be detected. With an increase of the sulfur content, however, it changes to the allotropic cubic CuZr B2 phase for the 2 mm $\text{CuZrS}_{1.0}$, $\text{CuZrS}_{2.0}$, and $\text{CuZrS}_{3.0}$ samples [Fig. 1(b)], thereby resulting in the formation of BMG composites solely containing the B2 phase. This finding indicates that proper addition of sulfur can destabilize the monoclinic phase, while facilitating the precipitation of the B2-CuZr phase. The reappearance of the monoclinic CuZr phase in the 3 mm $\text{CuZrS}_{1.0}$ sample [Fig. 1(c)], which experiences a slower cooling rate during casting than that of the 2 mm sample, further demonstrates the competitive relationship between the monoclinic and cubic CuZr phases and that the sulfur content influences it. Notably, further increase in sulfur content to $S \geq 3$ at.% leads to the precipitation of a $\text{Cu}_{10}\text{Zr}_7$ phase, displayed in the XRD patterns of the 3 mm $\text{CuZrS}_{3.0}$ [Fig. 1(c)] and 2 mm $\text{CuZrS}_{4.0}$ [Fig. 1(b)] samples. Hence, the increased precipitation tendency of the Cu-rich phase with rising sulfur levels should be accountable for the drastic reduction in GFA of the $\text{CuZrS}_{4.0}$ alloy. The underlying mechanism governing the stabilization of the low-temperature equilibrium phase will be discussed in Section 4. Another noteworthy phenomenon from the XRD results is that the crystalline product of the 3 mm $\text{CuZrS}_{2.0}$ sample is a single B2 phase [Fig. 1(c)], without the occurrence of the monoclinic CuZr and the orthorhombic $\text{Cu}_{10}\text{Zr}_7$ phases observed in the $\text{CuZrS}_{1.0}$ and $\text{CuZrS}_{3.0}$ samples. Manipulating the stability of different crystalline phases to achieve a competition balance was previously demonstrated to be an effective strategy for stabilizing the supercooled liquid and improving the GFA of multicomponent BMGs [13,39,40]. Herein, the slightly decreased GFA at sulfur content of ~ 2.0 at.%, as shown in Fig. 3, could be attributed to the absence of phase competition between various crystals. In other words, the precipitation tendency of the cubic CuZr phase may achieve a balance with that of the monoclinic CuZr and the orthorhombic $\text{Cu}_{10}\text{Zr}_7$ phases at the sulfur content of 1.0 and 3.0 at.%, respectively, thereby impeding the formation of each phase and leading to local maximums in GFA at these two compositions.

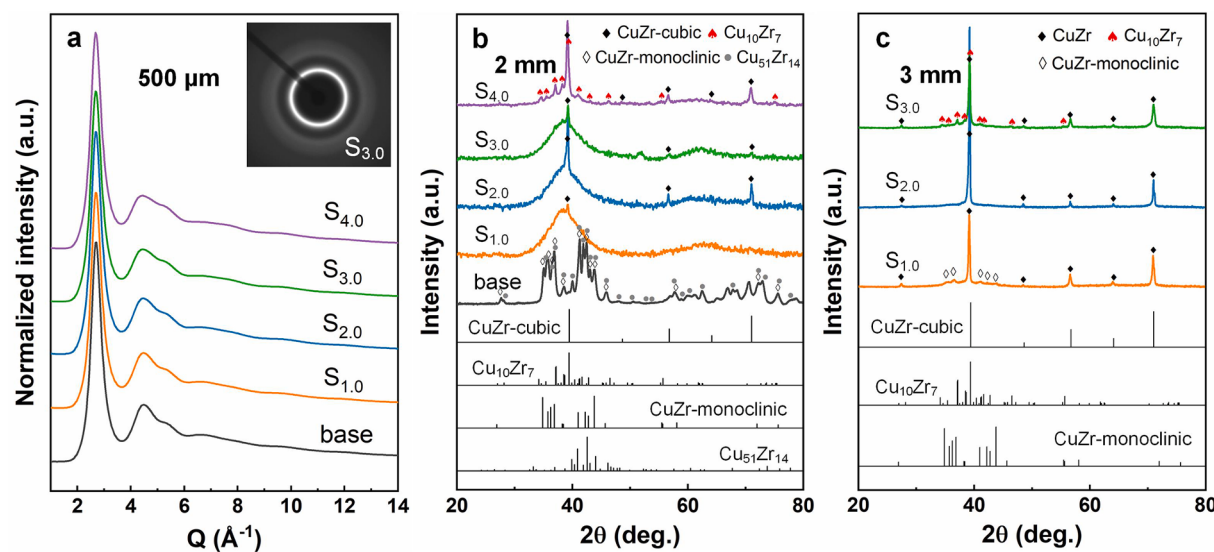


Fig. 1. X-ray diffraction results of $(\text{Cu}_{50}\text{Zr}_{50})_{100-x}\text{S}_x$ ($0 \leq x \leq 4.0$ at.%) samples with various geometries. (a) Synchrotron-based high-energy XRD patterns for plate-shaped samples with a thickness of 500 μm . Laboratory-based XRD patterns for rod-shaped samples with a diameter of (b) 2 mm and (c) 3 mm. The inset in (a) shows the raw 2D diffraction image of the $\text{CuZrS}_{3.0}$ sample. In (b) and (c), the standard diffraction patterns of the cubic CuZr , monoclinic CuZr , and $\text{Cu}_{10}\text{Zr}_7$ phases obtained from the PDF cards are displayed below the experimental results as a reference.

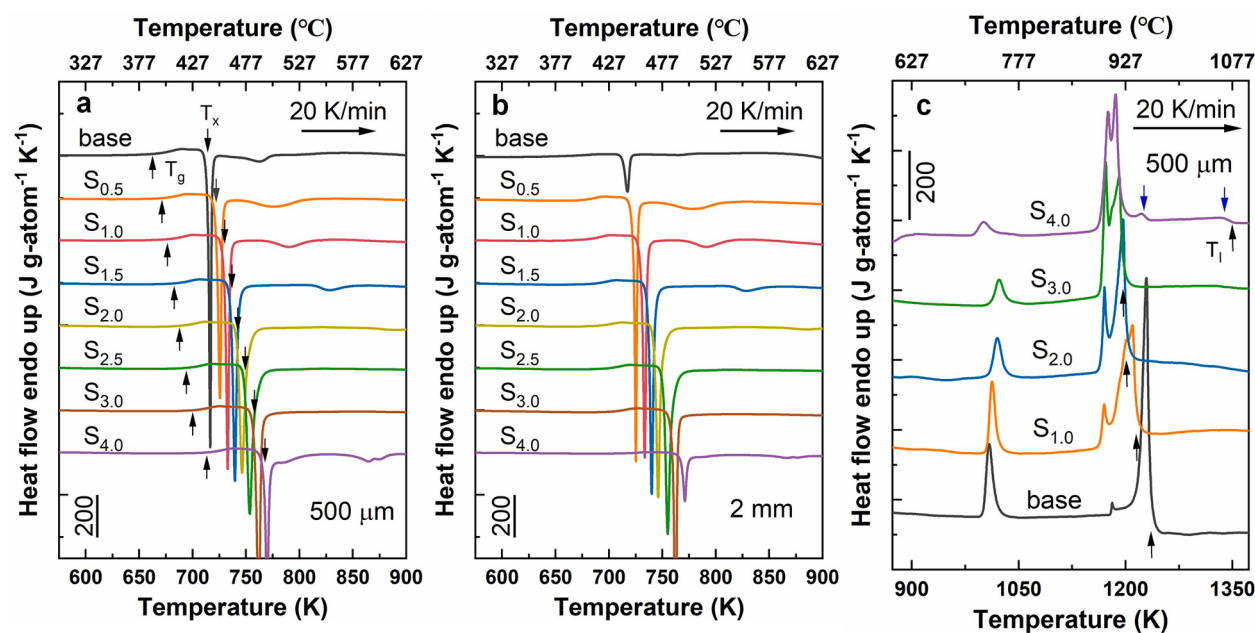


Fig. 2. DSC traces at 0.333 K/s of as-cast $(\text{Cu}_{50}\text{Zr}_{50})_{100-x}\text{S}_x$ ($0 \leq x \leq 4.0$ at.%) samples with different geometries: (a) 500 μm plates, (b) 2 mm rods. (c) High-temperature DSC scans up to 1373 K of as-cast plate-shaped samples with a thickness of 500 μm .

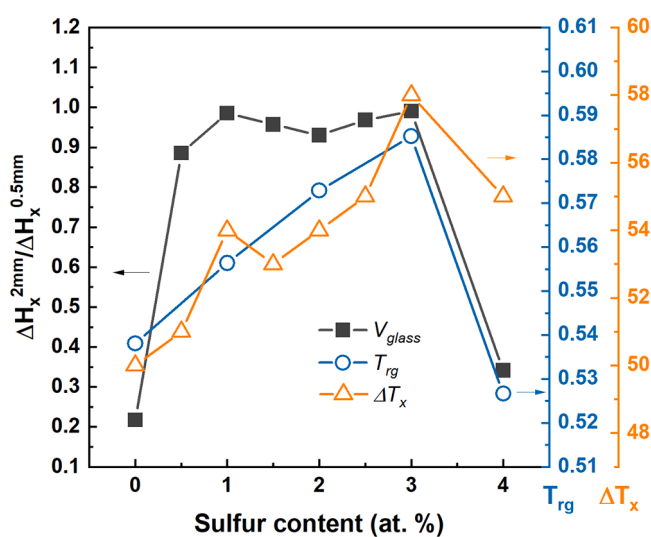


Fig. 3. Correlations between the GFA reflected by V_{glass} , thermal criteria T_{rg} and ΔT_x for the studied Cu-Zr-S alloys with different sulfur concentrations.

3.2. Thermal stability and crystallization behavior upon heating

Minor addition of sulfur was previously reported to significantly influence the crystallization behavior of BMGs [37]. Accordingly, a systematic investigation was conducted on the thermal stability and phase transformation behavior of the CuZrS_x BMGs upon heating. Fig. 2(a) and (c) show the low- and high-temperature DSC curves of the fully amorphous CuZrS_x samples at a heating rate of 0.333 K/s. The glass transition temperature, T_g , the onset temperature of crystallization, T_x , as well as the liquidus temperature, T_l , of the studied alloys are listed in Table 1. It is found that the T_g and T_x , marked by arrows in Fig. 2(a), increase continuously with rising sulfur content, indicating a significant slowdown of the liquid dynamics with sulfur incorporation in the glass and the deeply supercooled liquid in the vicinity of the glass transition. This finding is consistent with previous reports concerning the effect of sulfur on the stability of metallic liquids [35]. The width of the SLR, ΔT_x ($= T_x - T_g$), exhibits an increasing trend from 50 K of the base alloy to 58 K of the CuZrS_{3.0}, followed by a sharp decrease when the sulfur content reaches 4.0 at.% (Fig. 3). The reduction likely originates from the change of primary crystallization sequence during heating from the glass state. Furthermore, two local maxima in ΔT_x are reached at the sulfur content of 1.0 and 3.0 at.%, as shown in Fig. 3. This correlates well with the trend of the V_{glass} parameter, suggesting that the ΔT_x could be a qualitative indicator of the GFA of the studied alloy system. When looking at the high-temperature DSC curves displayed in Fig. 2(c), two distinct features can be recognized. First, the T_l temperature is

Table 1

Thermal parameters of 500 μm -thick CuZrS_x samples determined by low- and high-temperature DSC measurements at a heating rate of 0.333 K/s. The ΔH_x of the 2 mm rod samples is also included for comparison. The V_{glass} values are calculated as: $V_{glass} = \Delta H_x^{2\text{mm}}/\Delta H_x^{500\mu\text{m}}$.

Alloy	T_g (K)	T_x (K)	T_l (K)	ΔT_x (K)	T_{rg}	ΔH_s (J g-atom^{-1})	$\Delta H_x^{500\mu\text{m}}$ (J g-atom^{-1})	$\Delta H_x^{2\text{mm}}$ (J g-atom^{-1})	V_{glass}
Cu ₅₀ Zr ₅₀	664	714	1234	50	0.538	2640	5403	1049	19%
CuZrS _{0.5}	671	722	–	51	–	–	5390	4773	89%
CuZrS _{1.0}	676	730	1215	54	0.556	2248	5041	4968	99%
CuZrS _{1.5}	683	736	–	53	–	–	5130	4909	96%
CuZrS _{2.0}	688	742	1201	54	0.573	1679	5126	4769	93%
CuZrS _{2.5}	694	749	–	55	–	–	5072	4911	97%
CuZrS _{3.0}	700	758	1196	58	0.585	1198	4801	4755	99%
CuZrS _{4.0}	712	767	1352	55	0.527	885	4467	1525	34%

continuously shifted down from 1234 K to 1196 K with an increase of sulfur content to 3.0 at.%. For the alloy with 4.0 at.% of sulfur, however, a substantial increase in the T_l resulting from the occurrence of two subpeaks at considerably higher temperatures (blue arrows) than the main peak is clearly observed. This results in a drop of the reduced glass transition temperature, T_{rg} ($= T_g/T_l$), at the sulfur content of 4.0 at.%(Fig. 3). Second, the enthalpy of the solid phase transformation, DH_s , decreases with increasing sulfur concentration (Table 1), especially when the sulfur content exceeds 2.0 at.%. ΔH_s is the first endothermic peak in Fig. 2(c) at just above 1000 K. As introduced above, the corresponding microstructural evolution during the endothermic reaction is $Cu_{10}Zr_7 + CuZr_2 \xrightarrow{\text{cubic}} CuZr$. Therefore, the reduced DH_s observed implies a decreased volume fraction of the $Cu_{10}Zr_7$ and $CuZr_2$ phases in the crystallized samples, i.e., sulfur alters the crystallization products during heating from the glassy state.

In order to verify the sulfur-induced variation in crystallization products, *in-situ* HESXRD experiments (303–853 K) were conducted at 0.333 K/s to identify the structural evolution during the crystallization process of the base, $CuZrS_{1.0}$, and $CuZrS_{3.0}$ alloys (Fig. 4). The center panels of Fig. 4 [(b), (e) and (h)] show the contour plots of scattering intensity $I(Q)$ as a function of temperature. The DSC traces with the same heating rate [Fig. 4(a), (d) and (g)] are displayed vertically in the left window as a temperature reference of the diffraction data. To better visualize the phase transformation process upon heating, characteristic diffraction patterns, selected in accordance with the DSC results, are plotted in the right panel [Fig. 4(c), (f) and (i)]. As clearly exhibited by the 2D contour plots, Bragg reflections can only be observed once T_{x1} is reached, confirming the completely amorphous structure of the initial samples. For the base alloy [Fig. 4(a), (b) and (c)], the dominant crystalline phase during the principal crystallization event is identified as the (metastable) fcc-CuZr phase, which was previously observed in the $Cu_{47.5}Zr_{47.5}Al_5$ ($= (Cu_{50}Zr_{50})_{95}Al_5$)-based amorphous alloys [41]. The fcc phase decomposes into the equilibrium $Cu_{10}Zr_7$ and $CuZr_2$ phases upon further heating to temperatures above T_{x2} of ~ 750 K, demonstrating the metastable nature of the equiatomic fcc phase. Thus, the crystallization of the base alloy proceeds via a two-step route: Amorphous ($Cu_{50}Zr_{50}$) $\xrightarrow{\text{fcc}} CuZr \xrightarrow{\text{cubic}} Cu_{10}Zr_7 + CuZr_2$. As shown in [Fig. 4(d), (e) and (f)], the devitrification behavior of the $CuZrS_{1.0}$ is very similar to that of the base alloy. The system also experiences an intermediate metastable stage before reaching the thermodynamic equilibrium. The main difference is that Bragg peaks assigned to the $Cu_{10}Zr_7$ phase can already be observed during the primary crystallization stage. Therefore, the crystallization pathway of the $CuZrS_{1.0}$ alloy can be approximated as: Amorphous ($CuZrS_{1.0}$) $\xrightarrow{\text{fcc}} CuZr + Cu_{10}Zr_7 \xrightarrow{\text{cubic}} Cu_{10}Zr_7 + CuZr_2$. When the sulfur content reaches 3.0 at.%, however, significant variation in crystallization behavior can be detected. In the DSC scan, only a single exothermic event can be observed [Fig. 4(g)], and the contour plot of $I(Q)$ in Fig. 4(h) also indicates a one-step phase transformation process during heating. More importantly, a sulfide phase $Zr_{21}S_8$ is likely formed in the crystallized sample apart from the $Cu_{10}Zr_7$ and $CuZr_2$ phases. This finding explains the substantial decline of DH_s at $CuZrS_{3.0}$ [Fig. 2(c) and Table 1]. Furthermore, the observation of sulfide phase coincides with the findings by B. Adam [42] in Ti-Cu-Zr-S alloy system, where a Ti_8S_3 phase was found to precipitate first during devitrification. Overall, the crystallization sequence of the $CuZrS_{3.0}$ alloy upon annealing can be concluded as: Amorphous ($CuZrS_{3.0}$) $\xrightarrow{\text{Zr}_{21}S_8} Cu_{10}Zr_7 + CuZr_2$ without a significant formation of the intermediate metastable fcc-CuZr phase.

3.3. Atomic structure evolution upon sulfur incorporation

As shown in Fig. 5, the $S(Q)$ and $G(r)$ patterns were derived from the $I(Q)$ results to study the effect of sulfur on the atomic structure of the studied Cu-Zr-S alloys. The profiles in Fig. 5(a) and (b) are displayed one on the top of the other, thus visualizing the structural change upon sulfur incorporation. Clearly, the addition of sulfur leads to a continuous

decrease in intensity of the first and second $S(Q)$ peaks, as exhibited in Fig. 5(a). This phenomenon should originate from the fact that the scattering power of sulfur is significantly lower than that of the other two constituents, i.e., Cu and Zr. In Fig. 5(b), the 1st-5th $G(r)$ peaks are magnified in the insets to better present the structural evolution in real space. It is obvious that all peaks fade in intensity with increasing sulfur content. This is in line with the observed variations in $S(Q)$ profiles. Another noteworthy feature in $G(r)$ is that with the increase of sulfur concentration, the intensity at the high-r side of the first peak decreases drastically. According to the calculated weighting factors, W_{ij} , and the bond lengths, R_{ij} , of all possible atomic pairs, as listed in Table 2, the significant reduction in $G(r)$ at the high-r side is likely related to the change in the fraction of the Zr-Zr bond, which is one of the atomic pairs that contributes the most to the experimentally determined overall $G(r)$ curves.

The pair distribution function $g(r)$ is connected to the $G(r)$ via $g(r) = G(r)/4\pi r_0 + 1$, where r_0 is the average number density. In order to quantitatively determine the variation in bonding characteristics at the nearest-neighbor shell, the first $g(r)$ peak is fitted by three Gaussian functions representing the dominant Zr-Zr, Zr Cu and Cu-Cu atomic pairs (Fig. 6). The theoretical R_{ij} of the atomic pairs (see Table 2) is set as the initial peak centers for Gaussian fitting. As shown in Fig. 6 and Table 3, the area of the Zr-Zr peak continuously decreases with increasing sulfur content, while the other two peaks remain almost unchanged. In Fig. 6(d), the relative change of the Zr-Zr bond is calculated and compared to the relative reduction in the weight of the Zr-Zr atomic pair as a result of the incorporation of sulfur. It is obvious that the decreased fraction of the Zr-Zr bond ($\sim 11\%$) is significantly larger than the expected values determined from the weighting factor ($\sim 4\%$). These observations indicate that the microalloying element sulfur may prefer to combine with Zr, thus partially consuming the existent Zr-Zr bond in the Cu-Zr-based amorphous alloys. A similar phenomenon was reported previously in Cu-Zr-Al-S amorphous alloys. It was suggested that the reduction in the Zr-Zr fraction may originate from the fact that Zr is much less noble than Cu, thus easily bonding with the non-metallic element sulfur [37].

3.4. Mechanical properties of Cu-Zr-S alloys

The mechanical properties of the Cu-Zr-S BMG composites with a diameter of 2 mm were studied by room-temperature uniaxial compression tests conducted at a strain rate of $1 \cdot 10^{-4} s^{-1}$. The obtained engineering stress-strain curves are displayed in Fig. 7. The determined yield strength at an offset of 0.2% s_y , fracture strength s_f , Young's modulus E , and total strain until fracture e are summarized in Table 4. Since the base alloy shows distinct work softening just before fracture, the maximum strength s_{max} of the alloy is also listed in Table 4 as a supplement of the s_f . As can be seen, although the $Cu_{50}Zr_{50}$ composite exhibits considerable s_{max} of ~ 1.86 GPa and e of $\sim 12.6\%$, it yields even at the beginning of the mechanical test, completely losing the mechanical characteristic of BMGs. This behavior should arise from the fact that the 2 mm $Cu_{50}Zr_{50}$ cylindrical sample is severely crystallized. Interestingly, the B2 phase-containing $CuZrS_{1.0}$ sample shows a promising combination of high s_y , high s_f , and distinct plastic deformability reflected by the large e of $\sim 11.6\%$, which is obviously larger than the reported e values of 7.9 or 6.3% for $Cu_{50}Zr_{50}$ BMG with the same size [43,44]. The stress-induced martensitic transformation during compressive loading should account for the improved ductility of the B2 phase-reinforced BMG composites [23,25]. The ability to undergo yielding and plastic deformation draws a beautiful blueprint for the industrial application of the studied Cu-Zr-S BMG composites. This finding further proves that sulfur is of great use in the amorphous alloy community. When the sulfur content surpasses 1.5 at.%, however, excessive sulfur addition results in catastrophic fracture of the samples with no distinct yielding, as clearly exhibited in Fig. 7. The embrittlement effect by sulfur addition should be attributed to the inclusion of

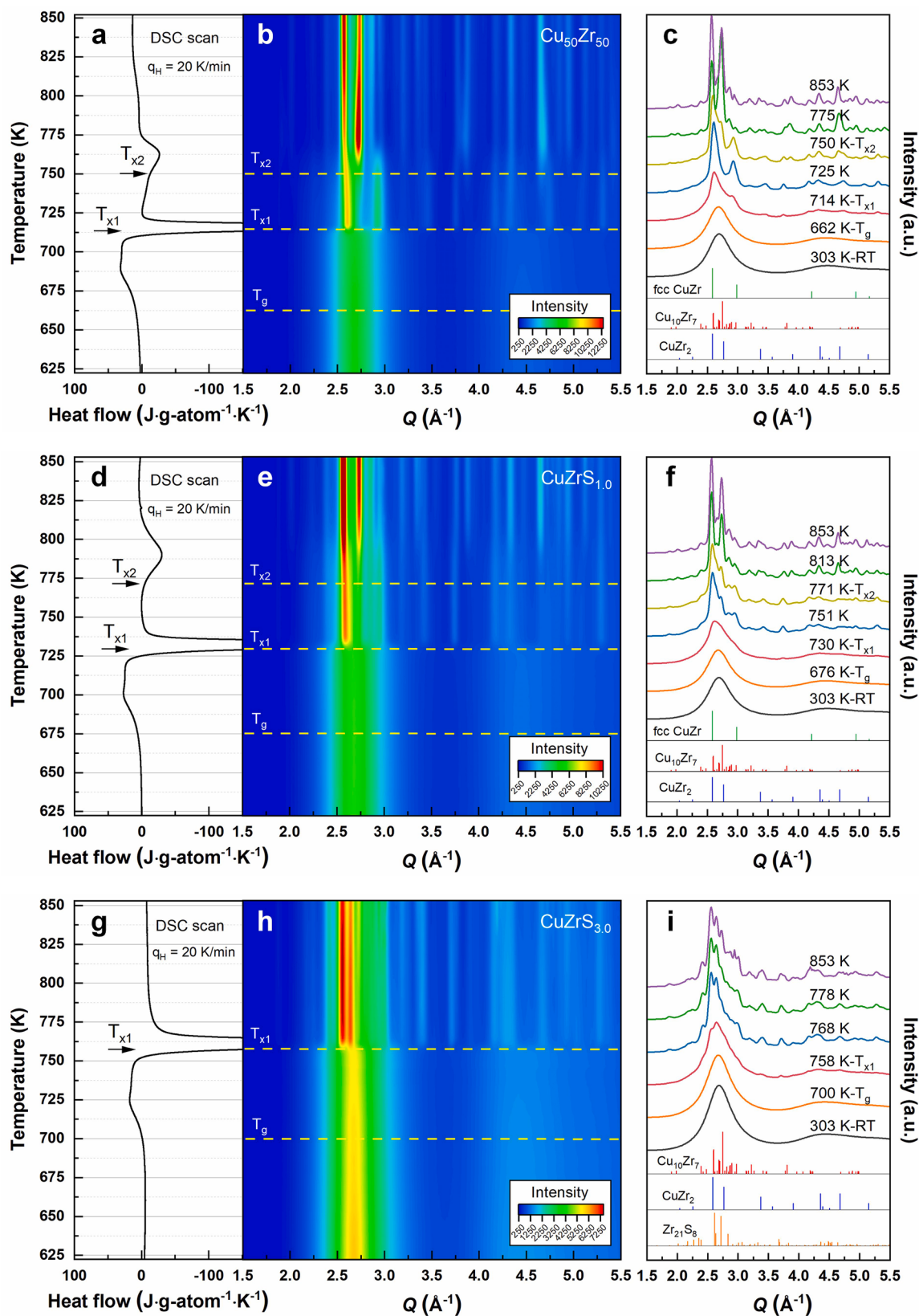


Fig. 4. Crystallization behavior of (a-c) $\text{Cu}_{50}\text{Zr}_{50}$, (d-f) $\text{CuZrS}_{1.0}$ and (g-i) $\text{CuZrS}_{3.0}$ glassy alloys upon heating. (a, d, g) DSC up-scan measured with the same heating rate as the synchrotron experiments. (b, e, h) Contour plots of diffraction intensity $I(Q)$, measured by *in-situ* HESXRD, as a function of temperature. (c, f, i) Selected $I(Q)$ patterns at different temperatures. The diffraction patterns of $\text{Cu}_{10}\text{Zr}_7$, CuZr_2 , fcc-CuZr and Zr_{21}S_8 phases, acquired from the PDF cards, are displayed at the bottom of (e, f, i) as a reference.

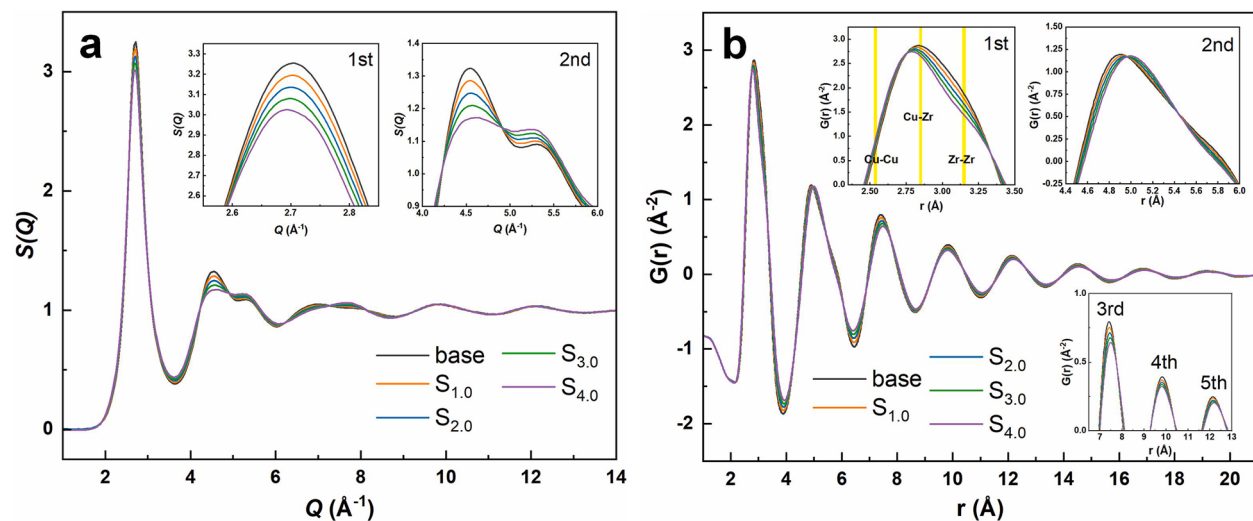


Fig. 5. HESXRD results of Cu-Zr-S amorphous alloys with different sulfur contents. (a) Structure factor $S(Q)$. (b) Reduced pair distribution function $G(r)$. The $S(Q)$ and $G(r)$ profiles are overlaid on the same scale, visualizing the structural change with sulfur alloying. The enlargement of the $S(Q)$ and $G(r)$ peaks is presented in the insets of (a) and (b).

Table 2

Bond Lengths, R_{ij} , and weighting factor, W_{ij} , of atomic pairs in the Cu-Zr-S amorphous alloys.

$i-j$	R_{ij} (\AA)	Weighting factor (W_{ij})				
		base	$S_{0.75}$	$S_{2.0}$	$S_{3.0}$	$S_{4.0}$
Zr-Zr	3.16	0.336	0.333	0.330	0.327	0.323
Zr-Cu	2.85	0.487	0.483	0.478	0.474	0.469
Cu-Cu	2.54	0.177	0.175	0.173	0.172	0.170
S-Zr	2.61	0	0.005	0.011	0.016	0.022
S-Cu	2.30	0	0.004	0.008	0.012	0.016
S-S	2.06	0	~0	~0	~0	~0

micro-pores (excessive sulfur easily causes micro-pores during casting) and the intrinsic bonding characteristics of sulfur [34,37].

4. Discussion

In our recent work, the effect of sulfur on the GFA of $\text{Cu}_{47.5}\text{Zr}_{45.1}\text{Al}_{7.4}$ BMG has been studied [37]. It was found that minor sulfur addition can improve the GFA of the ternary alloy, enhancing the critical casting size from 6 mm of the base alloy to 8 mm of the $\text{CuZrAlS}_{0.75}$. The increase in GFA is revealed to originate from the slowdown of liquid dynamics upon sulfur incorporation. This should also hold true for the studied binary alloy since a continuous increase in T_g and T_x with rising sulfur content can be observed in the DSC curves [Fig. 2(a)]. However, when the sulfur content exceeds a threshold value of 0.75 at.%, excessive sulfur induces the formation of a “big cube” $fcc-t_3$ phase ($\text{Zr}_{51}\text{Cu}_{28}\text{Al}_{21}$), which exhibits an extremely high nucleation rate, thus significantly deteriorating the GFA of the ternary Cu-Zr-Al alloy [37]. Obviously, the underlying mechanism resulting in the drop in GFA differs in the currently studied Cu-Zr-S system. The threshold value beyond which the GFA drops for the Cu-Zr binary alloy is located at the sulfur content of ~3.0 at.% (Fig. 3), which is significantly higher than that of the ternary alloy (0.75 at.%). In other words, the binary alloy without Al shows higher tolerance to the non-metallic element S compared to that of the Cu-Zr-Al alloy. This phenomenon is not surprising as the precipitation of the Al-rich fcc phase, which is catastrophic for the GFA, is avoided in the Cu-Zr-S system. As shown in Fig. 1(c), the crystalline phase leading to the sharp reduction of GFA in the high-sulfur Cu-Zr-S alloy transforms into the $\text{Cu}_{10}\text{Zr}_7$ phase. Herein, the question is why excessive sulfur facilitates the formation of the Cu-rich phase rather than the others. Clues

may lie in the change in atomic structure of the sulfur-containing alloys.

It was reported by Eckert et al. that oxygen in Zr-alloys likely combines with six Zr atoms to form atomic clusters in an octahedral configuration [45]. Considering that S is in the same group as O in the periodic table and has a strong electronegativity, it is natural to imagine that similar atomic clusters, i.e., sulfur atom is surrounded by six Zr atoms in the octahedral configuration as illustrated in Fig. 8(b), generate in the sulfur-bearing CuZr-based alloys. This conjecture conforms to the observed decreasing trend of the Zr-Zr fraction due to the incorporation of sulfur (Fig. 6), i.e., sulfur partially consumes the existent Zr-Zr bonds in the alloys. As presented in Fig. 8(b), the generation of the Zr-S clusters in the alloys will inevitably make the remaining matrix enriched in Cu. This might be the atomistic mechanism leading to the preferential precipitation of the $\text{Cu}_{10}\text{Zr}_7$ phase in the high-sulfur alloys since a small composition difference between the matrix and the Cu-rich phase will favor the precipitation of the $\text{Cu}_{10}\text{Zr}_7$ phase from the thermodynamic and kinetic perspectives of view [46,47]. Also, the existence of the Zr-S clusters may act as heterogeneous sites during the solidification of the alloy melts, thus accounting for the formation of the B2-CuZr phase which grows rather fast once nucleated [48]. Furthermore, the sulfur-containing clusters may destabilize the metastable fcc-CuZr phase formed upon heating, since S atom is too big for the fcc octahedral hole.

Although the effect of microalloying on the GFA and the B2 phase stability has been extensively studied in the past decades, elements that can simultaneously enhance the GFA and stabilize the formation of the B2 phase, thus improving the plasticity of BMGs, are rarely reported [49]. For example, B. Escher et al. [41] systematically studied the influence of Co and Ag on the GFA, phase transformation sequence, and mechanical properties of Cu-Zr-Al alloys. They found that the addition of Co can promote the formation of the B2 phase, making the alloy more plastic, but at the expense of the GFA. In contrast, the alloying of the noble element Ag can lead to significantly increased GFA but to reduced plasticity [41]. Considering that considerable effort has been put into finding industrially suitable microalloying components in the studied alloy system, the observation of simultaneously improved GFA and plastic deformability (B2 phase formation) by minor sulfur addition clearly demonstrates the high importance of sulfur in alloy development and properties modification. As an element with the characteristics of low cost, good availability, and non toxic modifications, sulfur shows high potential for industrial applications and is worth extending to different BMG-forming systems.

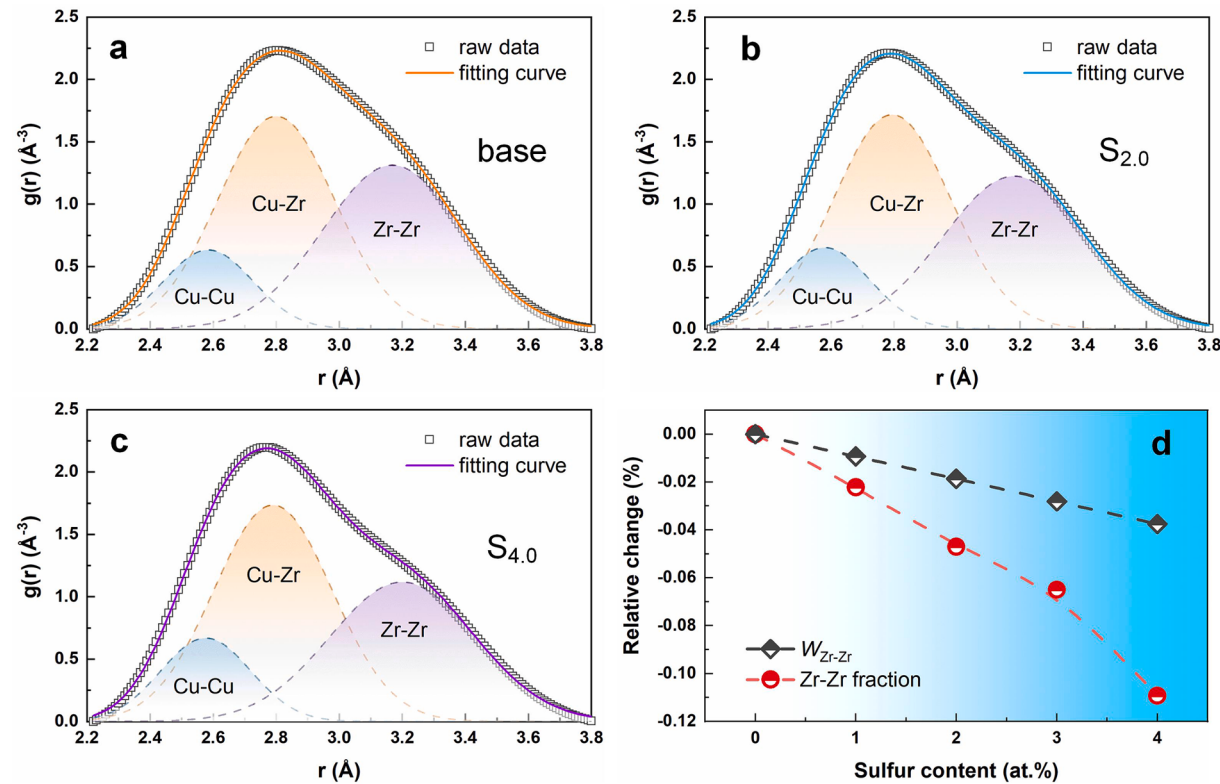


Fig. 6. Gaussian fitting results of the first $g(r)$ peak of the (a) base, (b) $\text{CuZrS}_{2.0}$ and (c) $\text{CuZrS}_{4.0}$ amorphous alloys. Only the three dominant atomic pairs, i.e., Zr-Zr, Zr-Cu and Cu-Cu, are considered for the Gaussian fitting. (d) The relative change in the Zr-Zr fraction and in the weight of the Zr-Zr bond of Cu-Zr-S alloys with different sulfur contents.

Table 3

The area of the Zr-Zr, Zr-Cu and Cu-Cu Gaussian peaks of Cu-Zr-S metallic glasses.

Atomic pair	Area base	$S_{0.75}$	$S_{2.0}$	$S_{3.0}$	$S_{4.0}$
Zr-Zr	0.723	0.707	0.689	0.676	0.644
Zr-Cu	0.793	0.796	0.801	0.804	0.817
Cu-Cu	0.224	0.227	0.231	0.231	0.238

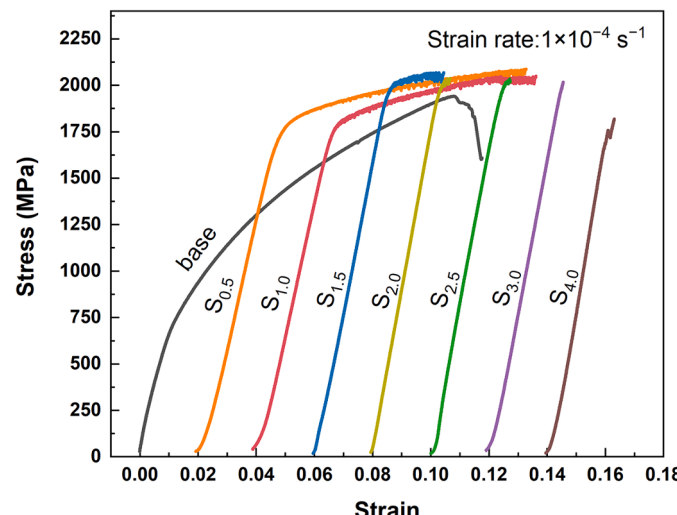


Fig. 7. Room-temperature compressive stress-strain curves of Cu-Zr-S BMG composites in 2 mm rod shape tested at a strain rate of $1 \times 10^{-4} \text{ s}^{-1}$.

Table 4

Room-temperature mechanical properties of 2 mm rod-shaped Cu-Zr-S BMG composites determined via uniaxial compression tests.

Alloys	σ_y (GPa) (0.2%)	σ_f (GPa) [σ_{\max}]	E (GPa)	ε (%)
$\text{Cu}_{50}\text{Zr}_{50}$ (amorphous) [43]	1.77	[1.88]	–	6.3
$\text{Cu}_{50}\text{Zr}_{50}$ (amorphous) [44]	1.27	[1.79]	84	7.9
$\text{Cu}_{50}\text{Zr}_{50}$ (crystallized)	–	1.46 ± 0.57 [1.86 ± 0.19]	–	12.6 ± 0.8
$\text{CuZrS}_{0.5}$	1.63 ± 0.16	2.11 ± 0.03	66.1 ± 6.2	10.8 ± 0.4
$\text{CuZrS}_{1.0}$	1.78 ± 0.08	2.05 ± 0.11	71.5 ± 1.6	11.6 ± 8.5
$\text{CuZrS}_{1.5}$	1.99 ± 0.04	2.03 ± 0.05	81.4 ± 0.4	3.5 ± 0.8
$\text{CuZrS}_{2.0}$	1.99 ± 0.07	2.06 ± 0.11	82.2 ± 3.3	0.7
$\text{CuZrS}_{2.5}$	2.01 ± 0.01	2.02 ± 0.02	82.1 ± 2.5	0.1
$\text{CuZrS}_{3.0}$	–	2.04 ± 0.09	83.6 ± 0.8	2.5 ± 0.1
$\text{CuZrS}_{4.0}$	–	2.00 ± 0.25	93.2 ± 2.7	2.3 ± 0.1

5. Conclusions

In summary, sulfur addition can significantly affect the GFA, the phase formation sequence, and the compressive mechanical properties of the $\text{Cu}_{50}\text{Zr}_{50}$ glass-forming alloy. Minor sulfur addition ($S \leq 3.0$ at.%) can improve the GFA and the stability of the B2-CuZr phase, thereby inducing the formation of sole B2 phase-contained BMG composites. The as-cast $\text{CuZrS}_{0.5}$ and $\text{CuZrS}_{1.0}$ BMG composites exhibit excellent plasticity with a total strain exceeding 10% under compression tests. The

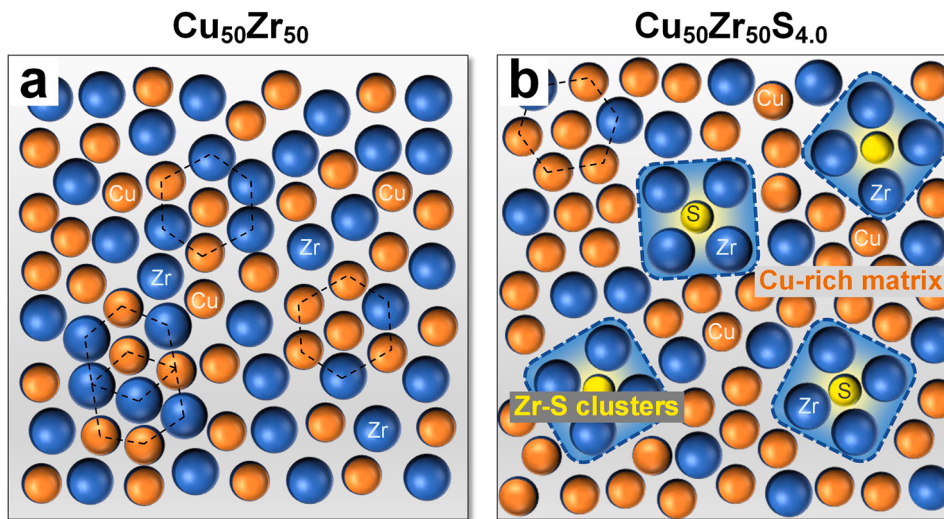


Fig. 8. Schematic diagrams illustrating the structural difference at atomic scale for the (a) Cu₅₀Zr₅₀ and (b) CuZrS_{4.0} amorphous alloys.

combination of high strength and distinct plastic elongation makes the Cu-Zr-S BMG composites very promising for industrial applications as structural materials. The threshold value of sulfur addition beyond which the GFA drastically decreases is revealed to locate at the sulfur content of ~3.0 at.%. The drop in GFA at $S > 3.0$ at.% should be attributed to the formation of the Cu₁₀Zr₇ phase during the solidification process. The atomistic investigation conducted by HESXRD reveals that sulfur tends to bond with Zr rather than Cu during alloying, resulting in the generation of Zr-S clusters and Cu-enriched matrix in the alloys. The formation of the Cu-rich regions explains why excessive sulfur induces the formation of the low-temperature equilibrium phase Cu₁₀Zr₇ during cooling. In addition, sulfur can alter the thermal stability and crystallization behavior of the studied alloy system upon heating. As the sulfur concentration increases to 3.0 at.%, a sulfide phase is found to precipitate preferentially during heating using the *in-situ* HESXRD technique. With the knowledge of the role of sulfur in affecting the crystallization sequence upon cooling from the top and during heating from the bottom, one can tailor the microstructure and properties of BMGs by manipulating the sulfur content. All in all, the findings in this work provide further evidence that sulfur is an effective microalloying element for BMGs. The development of sulfur-containing BMGs or BMG composites may accelerate the commercialization of metallic glasses.

Declaration of Competing Interest

The authors declare that they have no known competing financial interests or personal relationships that could have appeared to influence the work reported in this paper.

Acknowledgements

This work is partially supported by the German Research Foundation (DFG) through Grants No. BU 2276/10-1 and No. BU 2276/11-1. Moreover, we would like to acknowledge the financial support from Space Utilization System of China Manned Space Engineering (No. KJZ-YY-NCL08), Program 173 (No. 2020-JCIQ-ZD-186-01), the NSFC (Nos. 51925103, 51801027) and Shanghai Rising-Star Program Yangfan project (No. 23YF1411900). We want to thank Dr. B. Bochtler, B. Adam, L. Ruschel, S.S. Riegler, and Dr. W.F. Lu for many fruitful discussions and their experimental support. We acknowledge DESY (Hamburg, Germany), a member of the Helmholtz Association HGF, for the provision of experimental facilities. Parts of this research were carried out at PETRA III and we would like to thank Dr. A.-C. Dippel and Dr. S. Banerjee for their assistance in using beamline P21.1. H.R. Jiang would like to thank

China Scholarship Council (CSC) for providing a PhD scholarship.

References

- [1] D. Wang, Y. Li, B.B. Sun, M.L. Sui, Bulk metallic glass formation in the binary Cu-Zr system, *Appl. Phys. Lett.* 84 (2004) 4029–4031, <https://doi.org/10.1063/1.1751219>.
- [2] D. Xu, B. Lohwongwatana, G. Duan, W.L. Johnson, C. Garland, Bulk metallic glass formation in binary Cu-rich alloy series – Cu_{100-x}Zr_x (x=34, 36, 38.2, 40 at.%) and mechanical properties of bulk Cu₆₄Zr₃₆ glass, *Acta Mater.* 52 (2004) 2621–2624, <https://doi.org/10.1016/j.actamat.2004.02.009>.
- [3] T. Mei-Bo, Z. De-Qian, P. Ming-Xiang, W. Wei-Hua, Binary Cu-Zr bulk metallic glasses, *Chin. Phys. Lett.* 21 (2004) 901–903, <https://doi.org/10.1088/0256-307X/21/5/039>.
- [4] A. Inoue, Stabilization of metallic supercooled liquid and bulk amorphous alloys, *Acta Mater.* 48 (2000) 279–306, [https://doi.org/10.1016/S1359-6454\(99\)00300-6](https://doi.org/10.1016/S1359-6454(99)00300-6).
- [5] Y.C. Hu, H. Tanaka, Physical origin of glass formation from multicomponent systems, *Sci. Adv.* 6 (2020) eabd2928, <https://doi.org/10.1126/sciadv.abd2928>.
- [6] S. Ganorkar, S. Lee, Y.H. Lee, T. Ishikawa, G.W. Lee, Origin of glass forming ability of Cu-Zr alloys: a link between compositional variation and stability of liquid and glass, *Phys. Rev. Mater.* 2 (2018), 115606, <https://doi.org/10.1103/PhysRevMaterials.2.115606>.
- [7] Y. Li, Q. Guo, J.A. Kalb, C.V. Thompson, Matching glass-forming ability with the density of the amorphous phase, *Science* 322 (2008) 1816–1819, <https://doi.org/10.1126/science.1163062>.
- [8] T. Fujita, K. Konno, W. Zhang, V. Kumar, M. Matsuura, A. Inoue, T. Sakurai, M. W. Chen, Atomic-scale heterogeneity of a multicomponent bulk metallic glass with excellent glass forming ability, *Phys. Rev. Lett.* 103 (2009), 075502, <https://doi.org/10.1103/PhysRevLett.103.075502>.
- [9] C. Zhou, L. Hu, Q. Sun, J. Qin, X. Bian, Y. Yue, Indication of liquid-liquid phase transition in CuZr-based melts, *Appl. Phys. Lett.* 103 (2013), 171904, <https://doi.org/10.1063/1.4826487>.
- [10] L. Ward, D. Miracle, W. Windl, O.N. Senkov, K. Flores, Structural evolution and kinetics in Cu-Zr metallic liquids from molecular dynamics simulations, *Phys. Rev. B* 88 (2013), 134205, <https://doi.org/10.1103/PhysRevB.88.134205>.
- [11] Y.L. Sun, J. Shen, A.A. Valladares, Atomic structure and diffusion in Cu₆₀Zr₄₀ metallic liquid and glass: molecular dynamics simulations, *J. Appl. Phys.* 106 (2009), 073520, <https://doi.org/10.1063/1.3245324>.
- [12] H.L. Peng, M.Z. Li, W.H. Wang, C.Z. Wang, K.M. Ho, Effect of local structures and atomic packing on glass forming ability in Cu_xZr_{100-x} metallic glasses, *Appl. Phys. Lett.* 96 (2010), 021901, <https://doi.org/10.1063/1.3282800>.
- [13] H.R. Jiang, X.S. Wei, W.F. Lu, D.D. Liang, Z.H. Wen, Z. Wang, H.P. Xiang, J. Shen, Design of Cu-Zr-Al and Cu-Zr-Al-Sn bulk amorphous alloys with high glass-forming ability, *J. Non Cryst. Solids* 521 (2019), 119531, <https://doi.org/10.1016/j.jnoncrysol.2019.119531>.
- [14] G.J. Fan, M. Freels, H. Choo, P.K. Liaw, J.J.Z. Li, W.K. Rhim, W.L. Johnson, P. Yu, W.H. Wang, Thermophysical and elastic properties of Cu₅₀Zr₅₀ and (Cu₅₀Zr₅₀)₉₅Al₅ bulk-metallic-glass-forming alloys, *Appl. Phys. Lett.* 89 (2006), 241917, <https://doi.org/10.1063/1.2408634>.
- [15] A. Inoue, W. Zhang, Formation, thermal stability and mechanical properties of Cu-Zr and Cu-Hf binary glassy alloy rods, *Mater. Trans. JIM* 45 (2004) 584–587, <https://doi.org/10.2320/matertrans.45.584>.
- [16] W.H. Wang, Roles of minor additions in formation and properties of bulk metallic glasses, *Prog. Mater. Sci.* 52 (2007) 540–596, <https://doi.org/10.1016/j.pmatsci.2006.07.003>.

- [17] P. Yu, H.Y. Bai, M.B. Tang, W.L. Wang, Excellent glass-forming ability in simple Cu₅₀Zr₅₀-based alloys, *J. Non Cryst. Solids* 351 (2005) 1328–1332, <https://doi.org/10.1016/j.jnoncrysol.2005.03.012>.
- [18] A. Inoue, W. Zhang, T. Zhang, K. Kurosaka, High-strength Cu-based bulk glassy alloys in Cu-Zr-Ti and Cu-Hf-Ti ternary systems, *Acta Mater.* 49 (2001) 2645–2652, [https://doi.org/10.1016/S1359-6454\(01\)00181-1](https://doi.org/10.1016/S1359-6454(01)00181-1).
- [19] G. Duan, K. De Blauwe, M. Lind, J. Schramm, W. Johnson, Compositional dependence of thermal, elastic, and mechanical properties in Cu-Zr-Ag bulk metallic glasses, *Scr. Mater.* 58 (2008) 159–162, <https://doi.org/10.1016/j.scriptamat.2007.10.001>.
- [20] Q. Zhang, W. Zhang, A. Inoue, New Cu-Zr-based bulk metallic glasses with large diameters of up to 1.5cm, *Scr. Mater.* 55 (2006) 711–713, <https://doi.org/10.1016/j.scriptamat.2006.06.024>.
- [21] C.L. Dai, H. Guo, Y. Shen, Y. Li, E. Ma, J. Xu, A new centimeter-diameter Cu-based bulk metallic glass, *Scr. Mater.* 54 (2006) 1403–1408, <https://doi.org/10.1016/j.scriptamat.2005.11.077>.
- [22] Y. Chen, C. Tang, J.Z. Jiang, Bulk metallic glass composites containing B2 phase, *Prog. Mater. Sci.* 121 (2021), 100799, <https://doi.org/10.1016/j.pmatsci.2021.100799>.
- [23] Y. Wu, H. Wang, H.H. Wu, Z.Y. Zhang, X.D. Hui, G.L. Chen, D. Ma, X.L. Wang, Z. Lu, Formation of Cu-Zr-Al bulk metallic glass composites with improved tensile properties, *Acta Mater.* 59 (2011) 2928–2936, <https://doi.org/10.1016/j.actamat.2011.01.029>.
- [24] K. Song, D. Wu, S. Pauly, C. Peng, L. Wang, J. Eckert, Thermal stability of B2 CuZr phase, microstructural evolution and martensitic transformation in Cu-Zr-Ti alloys, *Intermetallics* 67 (2015) 177–184, <https://doi.org/10.1016/j.intermet.2015.08.015>.
- [25] S. Pauly, S. Gorantla, G. Wang, U. Kühn, J. Eckert, Transformation-mediated ductility in CuZr-based bulk metallic glasses, *Nat. Mater.* 9 (2010) 473–477, <https://doi.org/10.1038/NMAT2767>.
- [26] Y. Wu, Y. Xiao, G. Chen, C.T. Liu, Z. Lu, Bulk metallic glass composites with transformation-mediated work-hardening and ductility, *Adv. Mater.* 22 (2010) 2770–2773, <https://doi.org/10.1002/adma.201000482>.
- [27] H. Okamoto, Cu-Zr (Copper-Zirconium), *J. Phase Equilib. Diffus.* 29 (2008), <https://doi.org/10.1007/s11669-008-9267-2>, 204–204.
- [28] J. Schroers, Processing of bulk metallic glass, *Adv. Mater.* 22 (2010) 1566–1597, <https://doi.org/10.1002/adma.200902776>.
- [29] J. Schroers, On the formability of bulk metallic glass in its supercooled liquid state, *Acta Mater.* 56 (2008) 471–478, <https://doi.org/10.1016/j.actamat.2007.10.008>.
- [30] C. Zhang, D. Ouyang, S. Pauly, L. Liu, 3D printing of bulk metallic glasses, *Mater. Sci. Eng. R Rep.* 145 (2021), 100625, <https://doi.org/10.1016/j.mser.2021.100625>.
- [31] J. Wegner, M. Frey, M. Piechotta, N. Neuber, B. Adam, S. Platt, L. Ruschel, N. Schnell, S.S. Rieger, H.-R. Jiang, G. Witt, R. Busch, S. Kleszczynski, Influence of powder characteristics on the structural and the mechanical properties of additively manufactured Zr-based bulk metallic glass, *Mater. Des.* 209 (2021), 109976, <https://doi.org/10.1016/j.matdes.2021.109976>.
- [32] S. Floreen, J.H. Westbrook, Grain boundary segregation and the grain size dependence of strength of nickel-sulfur alloys, *Acta Metall.* 17 (1969) 1175–1181, [https://doi.org/10.1016/0001-6160\(69\)90095-9](https://doi.org/10.1016/0001-6160(69)90095-9).
- [33] D. Biká, J.A. Pfaendtner, M. Menyhard, C.J. McMahon, Sulfur-induced dynamic embrittlement in a low-alloy steel, *Acta Metall. Mater.* 43 (1995) 1895–1908, [https://doi.org/10.1016/0956-7151\(94\)00388-X](https://doi.org/10.1016/0956-7151(94)00388-X).
- [34] A. Kuball, B. Bochtler, O. Gross, V. Pacheco, M. Stolpe, S. Hechler, R. Busch, On the bulk glass formation in the ternary Pd-Ni-S system, *Acta Mater.* 158 (2018) 13–22, <https://doi.org/10.1016/j.actamat.2018.07.039>.
- [35] A. Kuball, O. Gross, B. Bochtler, R. Busch, Sulfur-bearing metallic glasses: a new family of bulk glass-forming alloys, *Scr. Mater.* 146 (2018) 73–76, <https://doi.org/10.1016/j.scriptamat.2017.11.011>.
- [36] A. Kuball, O. Gross, B. Bochtler, B. Adam, L. Ruschel, M. Zamanzade, R. Busch, Development and characterization of titanium-based bulk metallic glasses, *J. Alloys Compd.* 790 (2019) 337–346, <https://doi.org/10.1016/j.jallcom.2019.03.001>.
- [37] H.-R. Jiang, J.-Y. Hu, N. Neuber, B. Bochtler, B. Adam, S.S. Rieger, M. Frey, L. Ruschel, W.-F. Lu, A.-H. Feng, R. Busch, J. Shen, Effect of sulfur on the glass-forming ability, phase transformation, and thermal stability of Cu-Zr-Al bulk metallic glass, *Acta Mater.* 212 (2021), 116923, <https://doi.org/10.1016/j.actamat.2021.116923>.
- [38] X. Qiu, J.W. Thompson, S.J. Billinge, PDFgetX2: a GUI-driven program to obtain the pair distribution function from X-ray powder diffraction data, *J. Appl. Crystallogr.* 37 (2004) 678, <https://doi.org/10.1107/S0021889804011744>.
- [39] Y.J. Sun, D.D. Qu, Y.J. Huang, K.D. Liss, X.S. Wei, D.W. Xing, J. Shen, Zr-Cu-Ni-Al bulk metallic glasses with superhigh glass-forming ability, *Acta Mater.* 57 (2009) 1290–1299, <https://doi.org/10.1016/j.actamat.2008.11.007>.
- [40] Z.P. Lu, J. Shen, D.W. Xing, J.F. Sun, C.T. Liu, Binary eutectic clusters and glass formation in ideal glass-forming liquids, *Appl. Phys. Lett.* 89 (2006), 071910, <https://doi.org/10.1063/1.2336597>.
- [41] B. Escher, U. Kühn, J. Eckert, C. Rentenberger, S. Pauly, Influence of Ag and Co additions on glass-forming ability, thermal and mechanical properties of Cu-Zr-Al bulk metallic glasses, *Mater. Sci. Eng. A* 673 (2016) 90–98, <https://doi.org/10.1016/j.msea.2016.06.081>.
- [42] B. Adam, Characterization of a novel sulfur bearing titanium based bulk metallic glass, Master Thesis, Saarland University, 2020.
- [43] T.A. Baser, J. Das, J. Eckert, M. Baricco, Glass formation and mechanical properties of (Cu₅₀Zr₅₀)_{100-x}Al_x (x=0, 4, 5, 7) bulk metallic glasses, *J. Alloys Compd.* 483 (2009) 146–149, <https://doi.org/10.1016/j.jallcom.2008.07.147>.
- [44] J. Das, M.B. Tang, K.B. Kim, R. Theissmann, F. Baier, W.H. Wang, J. Eckert, Work-hardenable” ductile bulk metallic glass, *Phys. Rev. Lett.* 94 (2005), 205501, <https://doi.org/10.1103/PhysRevLett.94.205501>.
- [45] J. Eckert, N. Mattern, M. Zinkevitch, M. Seidel, Crystallization behavior and phase formation in Zr-Al-Cu-Ni metallic glass containing oxygen, *Mater. Trans. JIM* 39 (1998) 623–632, <https://doi.org/10.2320/matertrans1989.39.623>.
- [46] H.-R. Jiang, J. Tseng, N. Neuber, J. Barrirero, B. Adam, M. Frey, A.C. Dippel, S. Banerjee, I. Gallino, A.H. Feng, G. Wang, F. Mücklich, R. Busch, J. Shen, On the devitrification of Cu-Zr-Al alloys: solving the apparent contradiction between polymorphic liquid-liquid transition and phase separation, *Acta Mater.* 226 (2022), 117668, <https://doi.org/10.1016/j.actamat.2022.117668>.
- [47] R. Busch, F. Gärtnner, C. Borchers, P. Haasen, R. Bormann, Microstructure development during rapid solidification of highly supersaturated Cu-Co alloys, *Acta Metall. Mater.* 43 (1995) 3467–3475, [https://doi.org/10.1016/0956-7151\(95\)00038-W](https://doi.org/10.1016/0956-7151(95)00038-W).
- [48] I. Kaban, P. Jóvári, B. Escher, D.T. Tran, G. Svensson, M. Webb, T. Regier, V. Kokotin, B. Beuneu, T. Gemming, Atomic structure and formation of CuZrAl bulk metallic glasses and composites, *Acta Mater.* 100 (2015) 369–376, <https://doi.org/10.1016/j.actamat.2015.08.060>.
- [49] K.K. Song, S. Pauly, Y. Zhang, P. Gargarella, R. Li, N.S. Barekar, U. Kühn, M. Stoica, J. Eckert, Strategy for pinpointing the formation of B2 CuZr in metastable CuZr-based shape memory alloys, *Acta Mater.* 59 (2011) 6620–6630, <https://doi.org/10.1016/j.actamat.2011.07.017>.